ACS Partner Journal

CHEMICAL & BIOMEDICAL IMAGING

pubs.acs.org/ChemBioImaging

Perspective

Toward the Next Frontiers of Vibrational Bioimaging

Haomin Wang, Dongkwan Lee, and Lu Wei*

Cite This: *Chem. Biomed. Imaging* 2023, 1, 3–17

Read Online

ACCESS | Metrics & More | Article Recommendations

ABSTRACT: Chemical imaging based on vibrational contrasts can extract molecular information entangled in complex biological systems. To this end, nonlinear Raman scattering microscopy, mid-infrared photothermal (MIP) microscopy, and atomic force microscopy (AFM)-based force-detected photothermal microscopies are emerging with better chemical sensitivity, molecular specificity, and spatial resolution than conventional vibrational methods. Their utilization in bioimaging applications has provided biological knowledge in unprecedented detail. This Perspective outlines key methodological developments, bioimaging applications, and recent technical innovations of the three techniques. Representative biological demonstrations are also highlighted to exemplify the unique advantages of obtaining vibrational contrasts. With years of effort, these three methods compose an expanding vibrational bioimaging toolbox to tackle specific bioimaging needs, benefiting many biological investigations with rich information in both label-free and labeling manners. Each technique will be discussed and compared in the outlook, leading to possible future directions to accommodate growing needs in vibrational bioimaging.

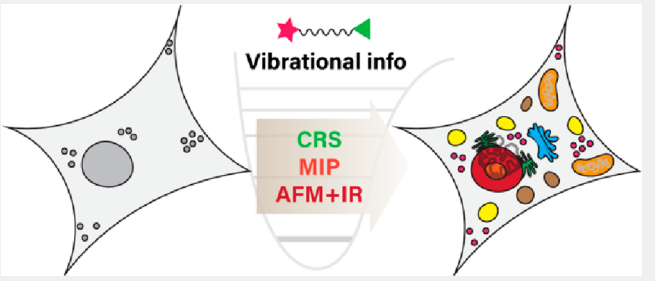

KEYWORDS: *Vibrational Spectro-microscopy, Coherent Raman Microscopy, Infrared Photothermal Microscopy, Atomic Force Microscopy, Vibrational Bioimaging*

INTRODUCTION

Raman and infrared (IR) are two well-established spectroscopic methods to unravel the vibrational information on molecules (Figure 1). As per selection rules, Raman detects vibrations with the changing polarizability, while IR detects vibrations with the changing dipole moment. In practice, chemical bonds in molecules that lack central symmetry (e.g., peptides and sugar chains) are usually active in both Raman and IR with different intensities.[1] The intrinsic bond-specific vibrational information is each molecule's distinctive "fingerprint" and serves as a molecular signature for chemical identification, permitting a nonintrusive way to identify bond-selective targets in complex biological environments.

Compared with fluorescence microscopy, vibrational microscopy lifts the need for large-fluorophore labeling and benefits from narrower vibrational bandwidth with no photobleaching issues. These advantages preserve the native states of biospecimens (especially for small biomolecules) for *in vivo* studies and promise supermultiplexity, which is limited to 4−5 colors in fluorescence microscopy.[2] However, conventional Raman and IR methods have severe limitations in modern microscopy applications. The spontaneous Raman (Figure 1a) is a weak process with cross sections of 10^{-28}∼10^{-30} cm^2; thus, it requires a long pixel dwell time for bioimaging and suffers from overwhelming backgrounds such as autofluorescence.[3] For common chemical bonds, IR cross sections are much higher than their Raman counterparts.[4] However, wavelength-dependent scattering in heterogeneous biological systems renders IR transmission/absorption measurements challenging. Additionally, IR imaging is hindered by poor spatial resolution (i.e., several μm) due to the diffraction limit of longer wavelengths and background absorptions in water. Therefore, modern vibrational imaging methods must find new ways to utilize the rich chemical information for advanced bioimaging applications.

The weak signal in spontaneous Raman is significantly boosted with coherent Raman scattering (CRS). CRS is a third-order nonlinear optical process that involves two pulsed laser beams with different colors named pump and Stokes[5] (ω_P and ω_S, $\omega_P > \omega_S$). Once the difference frequency matches the vibrational energy of the molecule ($\omega_p - \omega_S = \omega_\nu$), CRS processes, prominently the stimulated Raman scattering (SRS, Figure 1b) and the coherent anti-Stokes Raman scattering (CARS, Figure 1c), are intensified. Experimentally, SRS has demonstrated an up to an 10^8 times boost in cross sections compared to the spontaneous Raman conterpart,[3] thus allowing fast and sensitive bioimaging. Moreover, pump and

Received: January 7, 2023
Revised: March 3, 2023
Accepted: March 10, 2023
Published: March 28, 2023

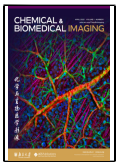

https://doi.org/10.1021/cbmi.3c00004
Chem. Biomed. Imaging 2023, 1, 3−17

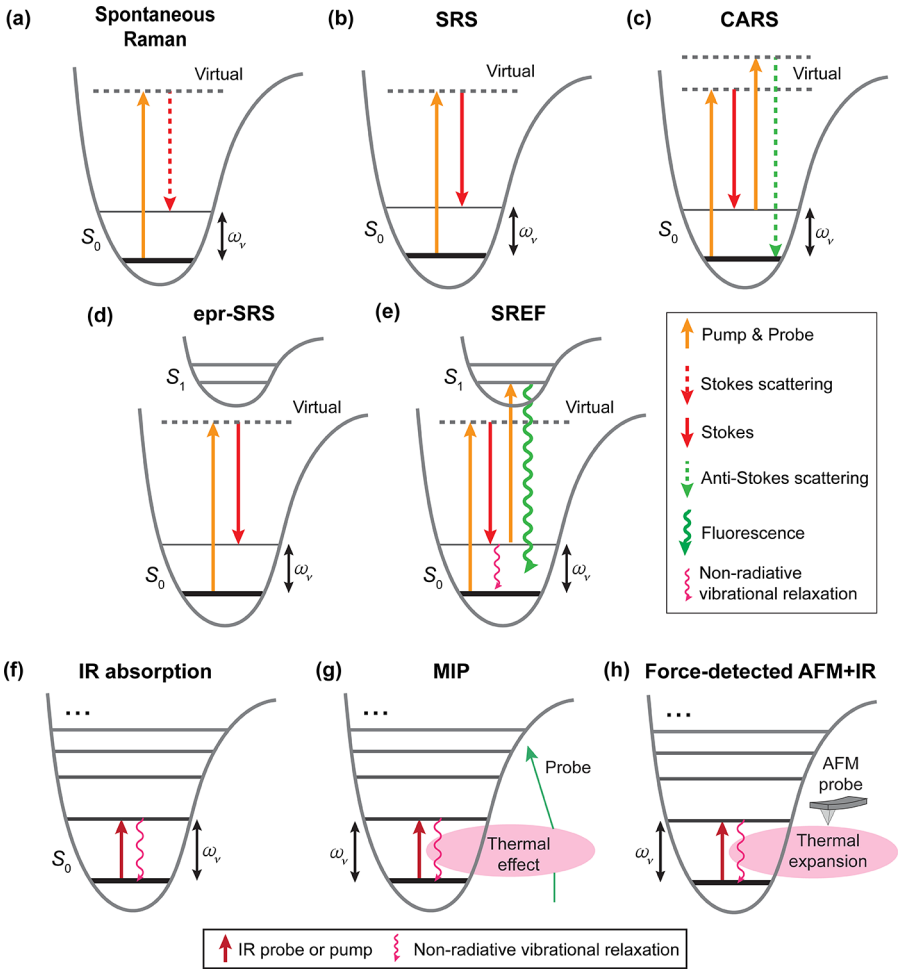

Figure 1. Energy diagrams of representative Raman and IR vibrational spectro-microscopy processes. (a–e) Energy diagrams of spontaneous Raman scattering (a), SRS (b), CARS (c), epr-SRS (d), and SREF (e). S_0 and S_1 are electronic ground and first excited states. ω_v is the vibrational energy. (f–h) Energy diagrams of linear IR absorption (f), MIP (g), and AFM-based force-detected photothermal microscopy (h).

Stokes beams are usually within the near-IR region, which induces little water absorption, much smaller phototoxicity, and penetrates deeper into thick tissues with intrinsic 3D sectioning than the visible light.[3]

In IR-based vibrational imaging, upon IR absorption, energy is transferred from photons into the sample and dissipates into thermal energy through nonradiative relaxations (Figure 1f). The IR-induced thermal energy generates various photothermal effects, such as temperature rise, refractive index change, photoacoustic wave generation, and photothermal expansion.[6] The magnitude of most photothermal effects is proportional to the absorbed IR energy. Therefore, instead of directly measuring IR transmission/absorption, one can use IR-induced photothermal effects to measure IR properties. Photothermal effects can be probed by an additional short-wavelength (e.g., visible to near-IR) laser (Figure 1g) through its intensity or phase changes, which has become the foundation of mid-infrared photothermal (MIP) microscopy,[7] also known as infrared photothermal heterodyne imaging (IR-PHI).[8]

Going beyond the far-field diffraction limit, nanoscale spatial resolution can be achieved through near-field effects from the tiny metallic probe in an atomic force microscope (AFM) (Figure 1h). The lightning rod effect from metal-coated AFM probes offers strong near-field enhancements, which reduces the excitation volume to a size comparable to the tip apex (e.g., 20 nm) and surpasses the diffraction limit.[9] Moreover, AFM cantilevers are sensitive force probes that detect instantaneous forces exerted by local photothermal expansions with high fidelity, enabling force-detected super-resolution IR microscopy without optical detectors.[10] Several AFM-based IR microscopies have been developed using this scheme, such as photothermal-induced resonance[11] (PTIR, or contact mode AFM-IR), photoinduced force microscopy[12] (PiFM), and peak force infrared (PFIR) microscopy.[13] Because the term "AFM-IR" was adopted early to designate PTIR with contact mode AFM,[14] we will use "AFM+IR" as a common name for these techniques throughout this Perspective.

In this Perspective, we first highlight the technical strengths of these three types of developing vibrational imaging modalities, CRS (SRS & CARS), MIP, and AFM-IR, from their experimental schemes to representative bioimaging applications. The pros and cons of each technique will be further discussed and compared. We seek to answer how to fully unleash the potential of each method for better vibrational imaging of biological systems and provide our perspectives on the future direction of these promising techniques.

https://doi.org/10.1021/cbmi.3c00004
Chem. Biomed. Imaging 2023, 1, 3–17

COHERENT RAMAN SCATTERING: SRS AND CARS MICROSCOPY

Introduction of SRS and CARS

SRS and CARS phenomena were initially used to shift laser frequencies and study coherent vibrational dynamics.[15] Fast and sensitive CRS bioimaging was not attainable until the dawn of ultrafast lasers.[16] In 1982, Duncan et al. reported the first demonstration of scanning CARS microscopy with synchronized picosecond dye lasers.[17] In 1999, the Xie group proposed a now widely used CARS configuration in a bioimaging platform.[18] Synchronized beams from a femtosecond optical parametric oscillator (OPO) were copropagated and tightly focused onto the sample, resulting in proper phase-matching conditions for an efficient CARS process. With high-intensity narrowband picosecond lasers, video-rate CARS imaging was demonstrated in 2005 on live mouse tissues.[19] The development of modern SRS microscopy followed in 2008, successfully eliminating the severe nonresonant background (NRB) issue in CARS for quantitative and straightforward detection analysis.[20−23] Utilizing the high-frequency (MHz) modulation transfer, the Xie group opened the biomedical SRS field with label-free imaging of living cells and tissues in 2008[21] and video-rate SRS imaging two years later.[24]

Mechanism of SRS and CARS Microscopy

Theories of SRS and CARS have been established in the literature.[5,25] In CARS, the new line at $2\omega_P - \omega_S$ is detected (Figure 1c). In SRS, either stimulated Raman loss (SRL) of the pump or stimulated Raman gain (SRG) of the Stokes pulses is detected (Figure 1b). It is essential to plot signal intensities detected by the photodetector (I_{SRS} or I_{CARS}) vs. the number (N) of probed oscillators (molecules):[26]

SRS (SRG or SRL)

$$I_{SRS} \propto 2\mathrm{Im}[\chi_R^{(3)}]I_P I_S \propto N I_P I_S \quad (1)$$

CARS

$$I_{CARS} \propto (|\chi_R^{(3)}|^2 + 2\chi_{NR}^{(3)}\mathrm{Re}[\chi_R^{(3)}] + |\chi_{NR}^{(3)}|^2)I_P^2 I_S \quad (2)$$

$$\chi_R^{(3)} \propto N \quad (3)$$

I_P and I_S stand for pump and Stokes intensities; $\chi_R^{(3)}$ and $\chi_{NR}^{(3)}$ are third-order susceptibilities of the materials from molecular vibrations and nonresonant backgrounds (NRBs), respectively.

The quadratic concentration dependence (when $\chi_{NR}^{(3)}$ is small) hinders CARS from conducting quantitative imaging and impedes its performance for analytes at low concentrations. In addition, the presence of NRB is often non-negligible, which distorts the spectral response and adds to unwanted backgrounds for imaging. Many efforts have been devoted to removing the NRB in CARS, however, at the expense of increasing experimental complexity.[27,28]

Thanks to the linear concentration dependence, SRS offers quantitative imaging. SRS is also free from NRB and analogous to spontaneous Raman, leading to straightforward signal interpretation. SRS detects small transmission changes in the pump or Stokes ($\frac{\Delta I}{I} = 10^{-7}\sim10^{-3}$) and benefits from a MHz modulation transfer scheme that suppresses the $1/f$ noise and reaches the shot-noise level for optimal signal-to-noise detection.[26] Compared with the NRB in CARS, backgrounds in SRS, such as cross-phase modulation, transient absorption, and the photothermal effect, are usually wavelength-independent and can be optimized through refractive index matching with careful sample preparation or be directly corrected.[29] Therefore, SRS is preferable for quantitative imaging of dilute biospecimens. The detection limit of SRS has reached the mM level for typical endogenous chemical bonds and the μM level for small alkynes in Raman-active molecular probes.[30]

Developments of SRS and CARS Microscopy in Bioimaging

Experimental Setup. The setups of SRS and CARS share many components and can be implemented together on the same microscope. A typical picosecond monochromatic SRS and CARS microscope is depicted in Figure 2a. Tunable sources that can output two series of synchronized pulses at ω_P and ω_S (e.g., an OPO driven by a mode-locked picosecond fiber laser) are used to provide narrowband excitation ($\omega_P - \omega_S$) with high spectral resolution (~10−15 cm^{-1}). Two pulses from the laser are first synchronized by a delay line and then combined and focused onto the sample plane with an

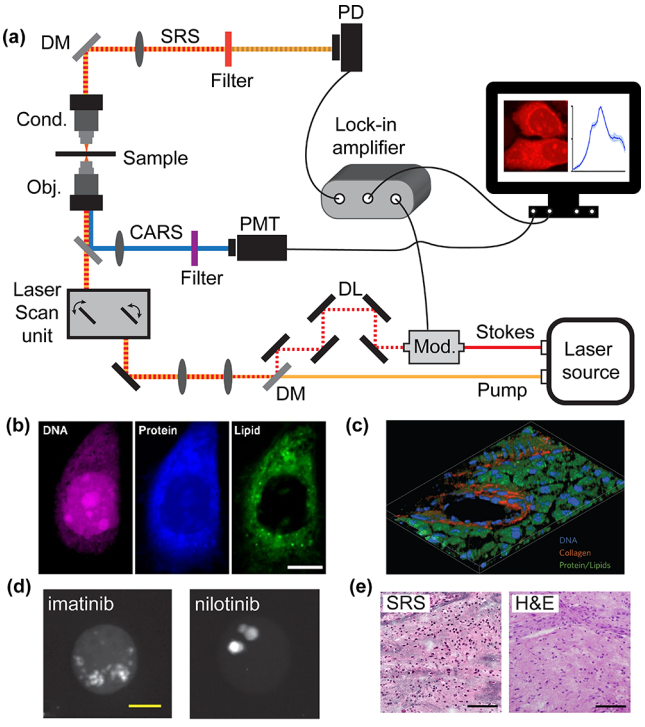

Figure 2. SRS and CARS microscopy. (a) A general setup for SRS and CARS microscopy. Mod. is a high-frequency modulator, usually an electronic optical modulator (EOM) or an acoustic optical modulator (AOM). The modulator is necessary for SRS but optional for CARS. DL: delay line for achieving temporal overlap of pump and Stokes. DM: dichroic mirror. Obj.: objective. Cond.: condenser. PMT: photomultiplier tube. PD: photodiode. (b) SRS images of a live HeLa cell in interphase. DNA (magenta), protein (blue), and lipids (green) are segregated by label-free imaging. Scale bar: 10 μm. Reprinted in part with permission from ref 35. Copyright 2015 National Academy of Sciences. (c) CARS Z-stack image of a murine pancreatic duct. Distributions of DNA (blue), collagen (orange), and protein/lipids (green) are revealed. Reprinted with permission from ref 32. Copyright 2014 Springer Nature. (d) SRS images of imatinib (left) and nilotinib (right) drugs enriched in BaF3/BCR-ABL1 cells. Scale bar: 5 μm. Adapted with permission from ref 33. Copyright 2014 Springer Nature. (e) SRS histology (left) and standard H&E staining (right) of tumor sections. Scale bars: 100 μm. Adapted with permission from ref 36. Copyright 2017 Springer Nature.

https://doi.org/10.1021/cbmi.3c00004
Chem. Biomed. Imaging 2023, 1, 3−17

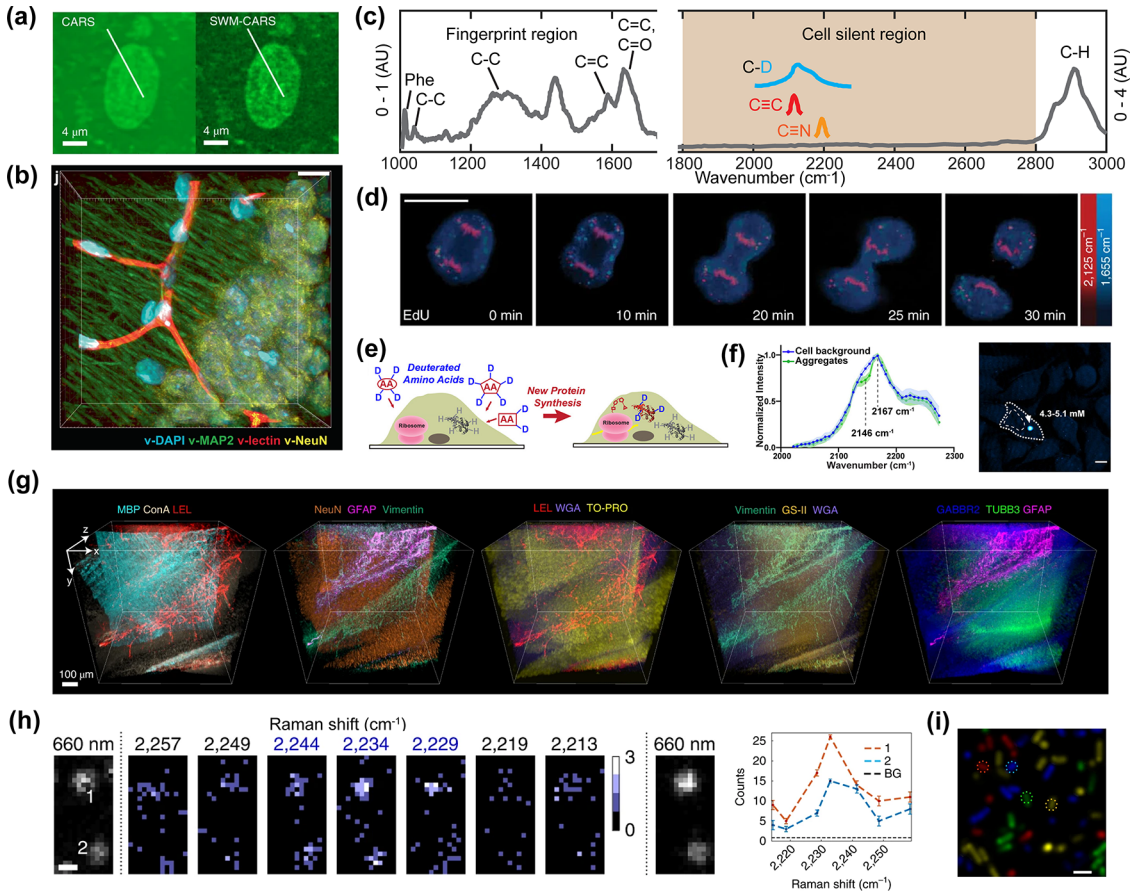

Figure 3. Developments of CRS microscopy toward bioimaging. (a) Regular CARS image (left) and higher-order CARS image (right, from six-wave-mixing CARS) of HeLa cells. Scale bars: 4 μm. Reprinted with permission from ref 49. Copyright 2019 The Authors. (b) Label-free three-dimensional VISTA prediction for nuclei (v-DAPI, cyan), dendrites (v-MAP2, green), vessels (v-lectin, red), and neuron cell bodies (v-NeuN, yellow) in a slice of mouse brain tissue. Scale bar: 40 μm. Reprinted with permission from ref 51. Copyright 2021 The Authors. (c) A typical Raman spectrum of mammalian cells. The vibrational frequency of common Raman probes falls into the cell-silent region with little background. Adapted with permission from ref 31. Copyright 2019 Springer Nature. (d) Time-lapse SRS images of a dividing cell labeled with 5-ethynyl-2′-deoxyuridine (EdU, a thymidine analogue with an alkyne group). Spatiotemporal distributions of EdU (red) and endogenous proteins (blue) are revealed. Scale bars: 10 μm. Reprinted with permission from ref 53. Copyright 2014 Springer Nature. (e) A cartoon showing the strategy of labeling live cells with deuterated amino acids to reveal *de novo* biosynthesis. Reprinted with permission from ref 30. Copyright 2016 The American Chemical Society. (f) Left: live-cell SRS spectra of C−D channel on mHtt-97Q aggregates with Gln-d_5 labeling (green) and cell backgrounds (blue). Right: quantitative SRS images of mHtt-97Q aggregates with Gln-d_5 labeling. Scale bar: 10 μm. Reprinted with permission from ref 55. Copyright 2020 The American Chemical Society. (g) Multiplexing volumetric SRS and fluorescence imaging of a 1 mm thick mouse cerebellum tissue with tissue clearing. A total of 11 targets are identifiable in the same region, enabling a spatial correlation study of 11 proteins. Reprinted with permission from ref 63. Copyright 2021 The Authors. (h) Fluorescence (gray) and frequency-swept SREF images (blue) of single rhodamine 800 molecules dispersed in PMMA films. Reconstructed SREF spectra at two single molecules and background are shown to the right. Scale bars: 400 nm. (i) Composite SREF image of living *E. coli* stained with four rhodamine 800 isotopologues. Four isotopologues are assigned different colors according to their vibrational frequencies. Scale bar: 2 μm. (h) & (i) are reprinted with permission from ref 76. Copyright 2019 The Authors.

objective. For SRS, one of the laser beams needs to be modulated at a high frequency (e.g., 20 MHz) to suppress the $1/f$ noise and increase the S/N through lock-in demodulation. A laser scanning unit can be implemented with a resonant galvo system to achieve fast imaging with a pixel dwell time down to the ns level.

The focal volume of CRS is defined by near-IR pump and Stokes foci, enabling the three-dimensional sectioning and achieving a typical lateral resolution of ∼400 nm and axial resolution of 1−2 μm.[31] Due to the coherent nature of the signals, the SRS signal is stronger in the forward detection geometry.[24] On the contrary, the CARS signal is generally obtained through epi-detection due to the ease of light collecting, but forward detection is also feasible. A large-area photodiode (PD) with a fast response to MHz modulation is commonly used in SRS detection; a photomultiplier tube (PMT) is frequently implemented with CARS for detecting anti-Stokes scatterings. Label-free SRS and CARS with narrowband excitation have been extensively applied for sensitive and selective biological and biomedical imaging (Figure 2b−e).[32−36]

Expansion of Spectral and Spatial Information. Various methods have been proposed to encode and extract more spectral information from CRS imaging by speeding up the laser tuning or utilizing broadband excitations and detections.[27] Multiplex CARS imaging has been demonstrated with broadband Stokes beams.[37,38] Multiplex SRS is achievable through rapidly tunable OPO,[39] pulse-shaping,[40] different modulation frequencies of multicolors,[41] or multichannel array detectors.[42] One of the elegant hyperspectral methods is

https://doi.org/10.1021/cbmi.3c00004
Chem. Biomed. Imaging 2023, 1, 3−17

spectral focusing, where a series of beat frequencies are generated as functions of the temporal delay between chirped pump and Stokes.[43,44] The fast tunability of spectral focusing has benefitted bioimaging applications such as revealing drug aggregations[33] (Figure 2d) and cancer metabolisms.[45]

Improving spatial resolution is another frontier to obtain more vibrational information. Inspired by the success of super-resolution fluorescence microscopy, Silva et al. utilized a toroidal-shaped decoherence beam in SRS and achieved subdiffraction limit resolution.[46] Based on saturation at high photon energies, saturation CARS has been demonstrated with higher spatial and spectral resolutions.[47] Similarly, saturation SRS has also achieved super-resolution in resolving mitochondria in live HeLa cells.[48] Besides depletion and saturation mechanisms, super-resolution is achievable by exploiting nonlinear power effects. By taking advantage of signal-laser power relations of the higher-order CARS process that involves higher vibrational levels (e.g., overtones), Gong et al. have achieved super-resolution with a smaller focal volume and reduced NRB[49] (Figure 3a).

Super-resolution is also obtainable if the samples are isotropically elongated and expanded in space. This principle sets the foundation for expansion microscopy (ExM), in which small structures in the sample are stretched evenly in 3D using polymer networks.[50] Qian & Miao et al. developed label-free super-resolution volumetric SRS imaging with a protocol termed VISTA and achieved a lateral resolution of 78 nm.[51] VISTA retains most endogenous proteins and removes excessive scattering lipids, optimizing conditions of cell and tissue samples for volumetric SRS imaging. Equipped with the machine-learning suite with the "ground truth" training data from immunolabeling fluorescence, VISTA provides label-free spatial predictions of the nucleus, blood vessels, neuronal cells, and dendrites in mouse brain tissues for multiplex imaging and microenvironment phenotyping with high accuracy[52] (Figure 3b).

Improvement of Sensitivity and Multiplexity. The detection limit of CRS microscopy for general endogenous chemical bonds in biological systems is only on the mM level. The aim for higher sensitivity has been a challenging task for CRS. Over the past decade, molecular-centric development has been catching up, significantly boosting the sensitivity and functionality of modern SRS microscopy. Introducing small bio- and spectrally orthogonal Raman probes offers enhanced sensitivity and specificity with maintained minimum perturbation, highly suited for live biological interrogations[3] (Figure 3c, i.e., the tags in the cell-silent region). For instance, the detection limit of SRS for an alkyne-labeled nucleoside analogue has reached 200 μM.[53] Compared with bulky fluorescent tags such as GFP, Raman labeling only requires a few chemical bonds into biomolecules, which do not alter the intrinsic functions of labeled biomolecules and enable biorthogonal chemical imaging.[30] The use of small Raman probes also allows dynamic tracking of biological processes (Figure 3d), which is not easily attainable with steady-state label-free imaging. For example, feeding the cell with deuterium-labeled amino acids can track the *de novo* protein biosynthesis dynamics across cells, neurons, and tissues[54] (Figure 3e). This strategy has been recently further tailored to provide unknown insights about the protein composition and concentration during the formation of intracellular protein aggregates in the live cellular model of Huntington's disease[55] (Figure 3f). Moreover, broad color palettes of Raman probes are obtainable with proper isotope chemical derivatizations.[56]

Physically, SRS can be further enhanced under electronic preresonance conditions. By tuning the pump frequency closer to the electronic absorption, electronic resonance can greatly promote vibrations coupled to the electronic transition, known as resonance Raman.[57] In SRS, the competition between enhanced vibrational signal and a featureless electronic background has to be balanced to reach an optimal signal-to-background ratio.[58] As a result, electronic preresonance SRS (epr-SRS, Figure 1d) with enhancement factors of more than 10^4 has reached a 250 nM detection limit for ATTO740.[59] Inspired by epr-SRS, multiple series of dye molecules and polymers have been engineered to achieve supermultiplexing vibrational imaging and functional sensing.[59−62] These engineered probes allow super multiplexity with tens of colors[63] (Figure 3g), superseding the fluorescence color barrier and promising a bright and colorful vibrational world.

Incorporating plasmonic enhancements such as in tip-enhanced Raman spectroscopy[64] (TERS) and surface-enhanced Raman spectroscopy[65] (SERS) is another way to enhance the Raman sensitivity. As a special case of SERS, TERS relies on localized surface plasmon resonance (LSPR)[66] of specialized (e.g., silver-coated) AFM probes. The collective oscillation of electrons induced in LSPR confines the incident light field into a nanoscale near-field around AFM probes with up to 10^8 signal enhancements[67] and leads to mode-specific vibrational imaging with atomic resolution.[68] For bioimaging, TERS has been used to collect *in situ* Raman signatures from biological species, including amyloid fibrils[69] in water and mammalian cell membranes.[70] Combining the SERS or TERS with coherent Raman excitation would in principle lead to even higher sensitivity. Using plasmonic enhancements brought by tiny crevices between gold nanoparticles and within a nanoantenna, single-molecule events have been recorded and analyzed by SRS[71] and CARS.[72,73] Furthermore, a stimulated TERS (sTERS) configuration has been established with a scanning tunneling microscope (STM) to obtain SRS spectra from monolayers.[74] While the plasmonic enhancement is promising for *in vitro* studies, the increased sample complexity and the possible spectral distortion make it challenging for general *in vivo* biological imaging.

On top of the epr-SRS, if an additional probe beam is involved, the dye molecule could be promoted to the electronically excited state (S_1) and then fluoresce (Figure 1e). The fluorescence intensity, in this case, is proportional to the population of vibrationally excited states.[75] This mechanism provides a new way to improve vibrational sensitivity by detecting background-free fluorescence, which bypasses the shot-noise detection scheme in SRS. In 2019, Xiong & Shi et al. developed stimulated Raman excited fluorescence (SREF) imaging with single-molecule sensitivity (Figure 3h) and multiplexing capability (Figure 3i).[76] SREF quickly demonstrated its unique advantages in a series of bioimaging tasks.[77] Similarly, the fluorescence-encoding and detection could be performed in the time domain with femtosecond lasers used in Fourier transform CARS. This modality, named fluorescence-encoded time-domain coherent Raman spectroscopy (FLETCHERS) was demonstrated by McCann et al. and found to increase the detection sensitivity by 1000 times.[78]

https://doi.org/10.1021/cbmi.3c00004
Chem. Biomed. Imaging 2023, 1, 3−17

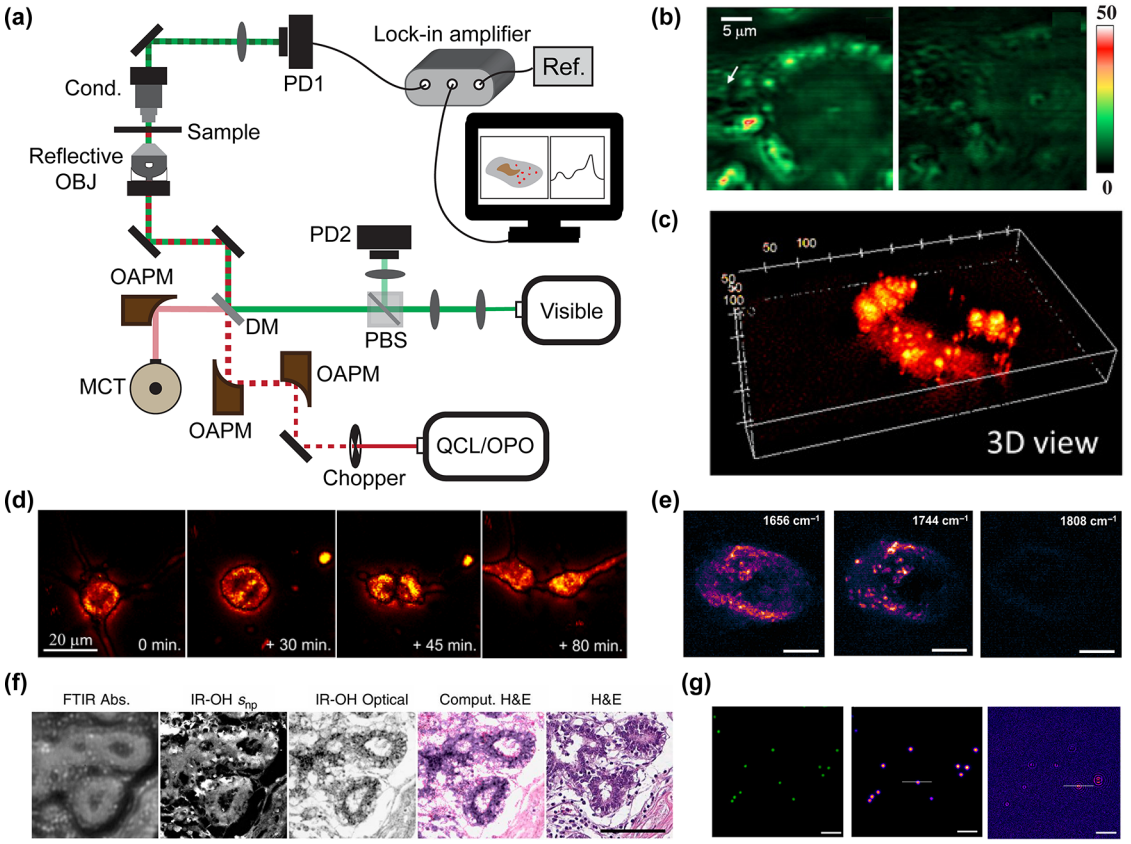

Figure 4. Mid-infrared photothermal microscopy. (a) Experimental scheme of a copropagating pump-probe MIP with forward detection. OAPM: off-axis parabolic mirror; DM: dichroic mirror; MCT: mercury-cadmium-telluride IR detector; PBS: polarizing beam splitter; PD: photodiode; OBJ: objective; Cond.: condenser; ref.: reference frequency. (b) MIP images of a preadipocyte 3T3-L1 acquired with IR excitation at 3.5 μm (left, on-resonance for lipids) and 3 μm (right, off-resonance). Reprinted with permission from ref 85. Copyright 2011 The Optical Society. (c) Reconstructed 3D view of PC-3 cells at the 1750 cm^{-1} C=O band, showing individual lipid droplets. Reprinted with permission from ref 7. Copyright 2016 The Authors. (d) The time course of cell division monitored every 5 min by MIP. Scale bar: 20 μm. Reprinted with permission from ref 86. Copyright 2019 The American Chemical Society. (e) Wide-field imaging of a living SKOV3 human ovarian cancer cell cultured on a silicon wafer. Acquired at 1656 cm^{-1} (protein), 1744 cm^{-1} (lipid), and 1808 cm^{-1} (off-resonance), respectively. Scale bars: 10 μm. Reprinted with permission from ref 87. Copyright 2019 The Authors. (f) Morphology-based inspection of tissues with IR-OH to generate stainless staining images that mimic the clinical practice. Scale bar: 100 μm. Reprinted with permission from ref 88. Copyright 2020 National Academy of Science. (g) (left) Fluorescence image of *S. aureus* deposited on a silicon substrate. (middle) Wide-field fluorescence-detected MIP image of the same cells with a 100-frame average. (right) Wide-field scattering-based MIP of the same field of view with a 100-frame average. Scale bars: 10 μm. Adapted with permission from ref 90. Copyright 2021 The American Chemical Society.

Midinfrared Photothermal Microscopy

MIP (or IR-PHI) overcomes the limitations of measuring transmission/absorption in direct mid-IR imaging.[79,80] Alternatively, IR-induced refractive index changes are probed by an additional visible probe beam in MIP (Figure 1g). MIP signals are usually extracted by demodulating the intensity change of the probe beam through a lock-in amplifier with a modulated IR beam at several to hundreds of kHz. The modulation ensures an optimal thermal effect to achieve a decent signal-to-noise (S/N) ratio.[7] Compared with traditional IR microscopy, MIP poses several strengths for bioimaging. First, the spatial resolution in MIP is usually determined by the diffraction limit of the visible probe beam, which is much higher than the long-wavelength IR. The reported lateral and axial resolution in MIP have reached ~300 nm and ~1.5 μm, respectively.[8,81] The spatial resolution could be further improved to the super-resolution regime (~120 nm) by differentiating the spatially heterogeneous photothermal response in the temporal domain through high-harmonic lock-in demodulation.[82] Second, MIP provides reduced water background. As water holds a large heat capacity, only a small change in the temperature, reflected in a slight change in refractive index, can be induced by IR radiations. Third, the pump-probe mechanism in MIP allows 3D optical sectioning for volumetric imaging. Fourth, the indirect probing approach avoids the wavelength-dependent scattering in the direct absorption, which is desired in imaging heterogeneous samples.

Experimental Setup

Nanosecond optical parametric oscillator (OPO) output or the more popular quantum cascade lasers (QCLs) are generally used in MIP with narrowband radiation.[79] CW visible or near-IR lasers are often used as the probe beam, and their intensity change is detected by photodiodes. Figure 4a shows a typical copropagating scheme, where the IR pump and the visible probe beams are combined at a dichroic mirror and then focused together onto the sample. Due to the large wavelength difference between the two beams, a reflective objective is used to avoid chromatic aberrations. As reflective lenses have limited numerical aperture (NA) compared to refractive ones, the spatial resolution is relatively less satisfying with the

https://doi.org/10.1021/cbmi.3c00004
Chem. Biomed. Imaging 2023, 1, 3−17

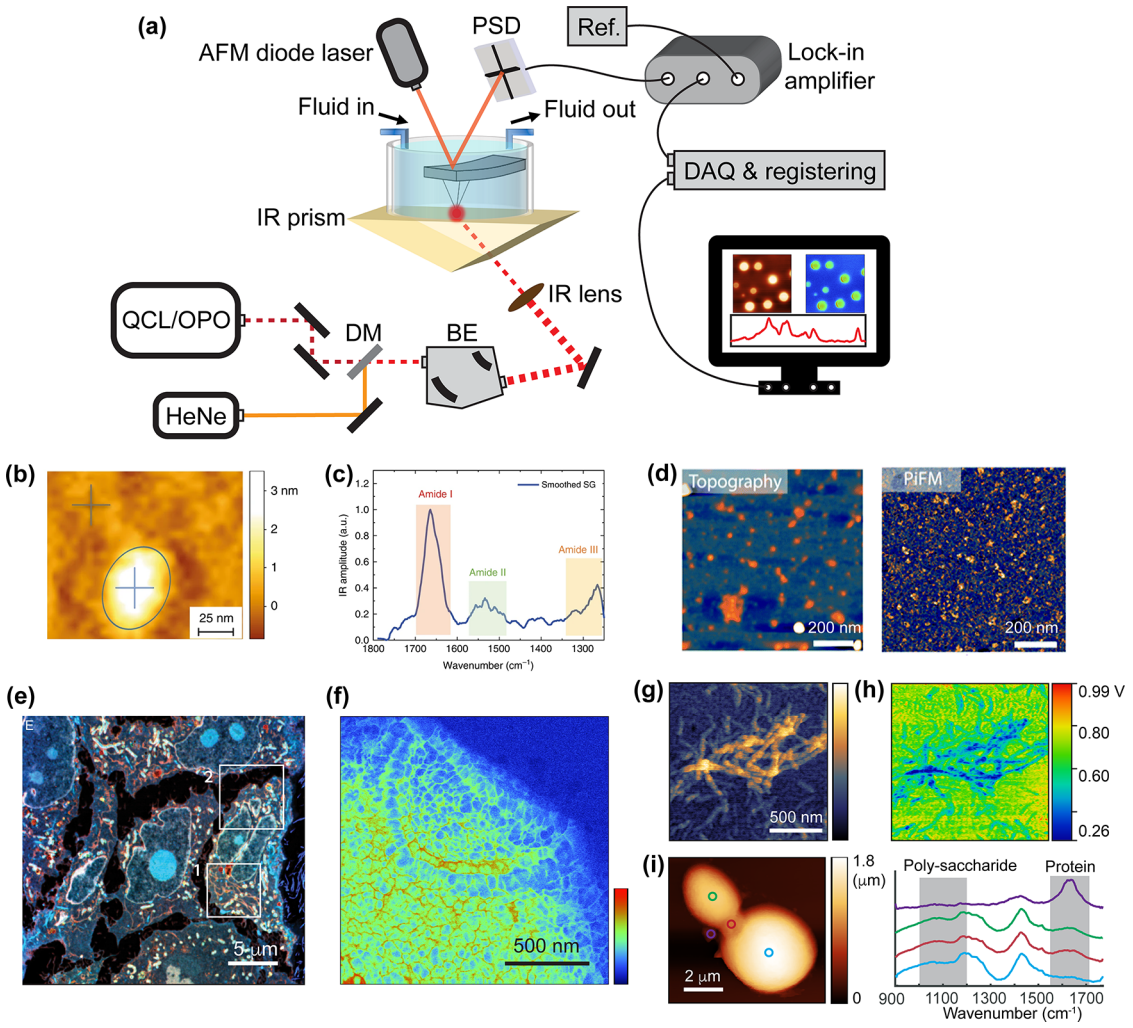

Figure 5. Experimental setup and applications of force-detected AFM+IR. (a) A typical AFM+IR experimental setup for bioimaging. DM: dichroic mirror; BE: reflective beam expander; PSD: position-sensitive detector; ref.: reference frequency; DAQ: data acquisition. (b,c) AFM topography (b) and PTIR spectra (c) of a single thyroglobulin molecule (indicated with a circle in topography) on gold. Amide I, II, and III bands are revealed in PTIR spectra from the single protein molecule. Reprinted with permission from ref 100. Copyright 2020 The Authors. (d) AFM topography (left) and PiFM image (right) at 1529 cm^{-1} of particles of the biotoxin abrin toxin (ABR) on mica. Individual protein particles are highlighted in the PiFM image. Reprinted with permission from ref 112. Copyright 2019 Royal Society of Chemistry. (e) Composite AFM-IR image (red: 990 cm^{-1}, green: 1550 cm^{-1}, blue: 1660 cm^{-1}) of fine ultrastructures in MCF-10A cells. Reprinted with permission from ref 103. Copyright 2022 The Authors. (f) PFIR image (bottom) at 1030 cm^{-1} (polysaccharide) of the bud scar region on the surface of yeast (*Saccharomyces cerevisiae*) cell wall, revealing the nanoscale ultrastructure. Reprinted with permission from ref 118. Copyright 2020 The American Chemical Society. (g,h) PFIR image at 1659 cm^{-1} (g) and KPFM surface potential image (h) of deposited FapC amyloid fibrils on silicon substrate under neutral pH. The correlative mapping between IR and surface potential unravels the relationship between secondary structures and the electric properties of amyloid fibrils. Reprinted with permission from ref 116. Copyright 2020 John Wiley and Sons. (i) AFM topography (left) of a yeast cell wall particle immersed in D_2O and PFIR spectra (right) obtained from four spots indicated in the topography. Differences in IR absorptions indicate the presence of protein components (purple) close to the septum of two dividing yeast cells. Adapted with permission from ref 119. Copyright 2021 The American Chemical Society.

copropagating geometry. MIP can also work with counter-propagating geometry, where the probe beam can be focused more tightly with a separate high-NA refractive objective to achieve higher resolution with an optical alignment of increased complexity. Both geometries require IR-transparent substrates (e.g., CaF_2, ZnSe, Si, and Ge) to allow a high IR transmission. In addition to the forward transmission detection (Figure 4**a**), the probe beam can also be detected in epi-mode with a quarter waveplate and a polarizing beam splitter.[79]

Development of MIP in Bioimaging

The thermal lens effect with electronic excitation has been exploited for optical imaging down to single-molecule sensitivity.[83] Lee et al. were the first to demonstrate photothermal imaging using a mid-IR vibrational pump.[84] With a near-IR probe from an OPO output, MIP images of oil droplets in water were acquired at two different IR frequencies corresponding to the CH_2 stretching mode of oil and OH stretching of water, indicating the chemical specificity of the technique. Later, the authors also demonstrated MIP imaging in preadipocyte 3T3-L1 cells using a 633 nm probe beam[85] (Figure 4b).

In 2016, utilizing the broadly tunable QCL with a 100 kHz repetition rate, Zhang et al. developed a volumetric MIP imaging platform and achieved bioimaging of live cells and organisms *in vivo*.[7] A 785 nm CW laser was coaligned with the

https://doi.org/10.1021/cbmi.3c00004
Chem. Biomed. Imaging 2023, 1, 3−17

QCL in the copropagating scheme. To increase the S/N ratio, signals from the detector were first filtered by a resonant amplifier before being sent to the lock-in amplifier. A dark-field objective was used to better detect the change in the probe intensity. The detection limit of C=O bonds in valerolactone was shown to be 10 μM. Using MIP, a 3D map of lipid distributions in a PC-3 cell has been obtained (Figure 4c). This work accelerated the commercialization of MIP[80] and opened up a wide range of possibilities in investigating biological systems in mid-IR with subcellular resolution. With a similar setup, Lim et al. demonstrated time-lapse MIP imaging of live brain cells,[86] providing structural and chemical information during cell division (Figure 4d).

To tackle the imaging speed limit for tracking fast dynamics, Bai et al. demonstrated wide-field MIP imaging at a frame rate up to 1250 frames/s and an illumination area of 36 × 36 μm^2 using a customized lock-in camera and realized bond-specific imaging of proteins and lipids in live ovarian cancer cells cultured on a silicon wafer[87] (Figure 4e). Similarly, Schnell et al. developed IR-optical hybrid (IR-OH) imaging using a wide-field interferometric approach.[88] By combining the molecular and morphological information from IR and brightfield images, the authors demonstrated the all-computational staining that may remove the need for chemical stains in histopathology (Figure 4f).

Although the IR cross section is a few orders of magnitude larger than that of Raman, the intensity change of the probe beam caused by the photothermal effects is still small, near 10^{-4} K^{-1} for most materials. To increase the MIP sensitivity, a larger modulation depth is required. To this end, Li et al. and Zhang et al. independently developed fluorescence-detected MIP microscopy, which labels the sample with fluorescent dyes and detects fluorescence changes induced by IR absorptions of endogenous biomolecules (e.g., proteins and lipids).[89,90] The probe beam here serves as an excitation light to generate fluorescence. The modulation depth of fluorescence-detected MIP was found to be 100 times larger than that of the regular scattering. As a result, improved S/N ratios higher than the regular MIP have been demonstrated in both stage-scan and wide-field imaging (Figure 4g).

AFM-BASED IR-PHOTOTHERMAL MICROSCOPY

Emergence of AFM-Based Vibrational Microscopy

The invention of STM by Binnig and Rohrer stunned the world with images of single atoms in the 1980s.[91] Soon after, a host of scanning probe microscopy (SPM) methods were developed and benchmarked, which revolutionized the advancement of nanotechnology. One of the most versatile SPM methods is atomic force microscopy (AFM).[92] AFM uses a sharp tip fixed to the end of a cantilever to scan the sample surface. The cantilever (usually hundreds of μm long with force constants of a few N/m) acts as a soft spring to read out small mechanical forces between the tip and the sample.[93] The spatial resolution of AFM depends on the tip geometry and has already achieved single-atom imaging in early demonstrations.[94]

Scientists have devoted many efforts to combining AFM with light to make optical imaging far below the diffraction limit possible. One successful strategy is to use the AFM tip as a tiny optical emitter. The idea now evolves into the field of near-field optics, where a metal-coated AFM tip acts as a nanoantenna to greatly confine and enhance local light fields due to LSPR.[66] For example, TERS has achieved remarkable single-molecule resolution in imaging specific vibrational modes.[68] However, TERS operation requires extensive expertise, and the tip coating remains a bottleneck for reproducible imaging.[95] For IR spectro-microscopy, near-field illumination is attainable with scattering-type scanning near-field optical microscopy[96] (s-SNOM). s-SNOM utilizes plasmonic tip enhancements in mid-IR and detects scattered light from the tip-sample region with 20 nm resolution.[97] However, s-SNOM requires complex interferometric detection and multiple laser sources to retrieve IR absorption profiles. In this Perspective, we will focus on force-detected AFM+IR methods for bioimaging.

AFM-Based Force-Detected Photothermal Microscopy

Experimental Setup. Instead of using an optical probe in MIP, IR-induced vibrational information could be recovered with high fidelity through AFM cantilever force detection. Transient local photothermal expansion induced by IR absorption can "kick" up the cantilever and cause it to vibrate. Consequently, the cantilever could be modeled as a driven damped oscillator and used to measure the magnitude of photothermal expansion from IR absorption (Figure 1h), which is directly correlated with the IR cross section (σ_{abs}) of the sample. The induced oscillation amplitude (A) of the cantilever follows:[98]

$$A \propto NC_{cant}C_{exp}C_{th}\sigma_{abs}I_P \tag{4}$$

in which N is the number of absorbers, C_{cant} is the cantilever contribution depending on its force constant, mechanical eigenmodes, etc., C_{exp} designates contributions from samples' thermal expansion, C_{th} is the contribution from local thermal dynamics (e.g., heat dissipation), and I_P is the pump energy of incident light.

A typical setup for force-detected AFM+IR is depicted in Figure 5a. A pulsed mid-IR laser source (QCL or OPO with repetition rate from kHz to MHz) is collimated and focused on the tip-sample region. A visible guide laser (e.g., HeNe) is often aligned collinearly with IR for easier alignment. A total internal reflection (TIR) illumination scheme is shown in Figure 5a, where an IR-transparent TIR prism (e.g., Si, Ge, and ZnSe) is used as the AFM substrate. A fluid cell could be installed on top of the TIR prism to map biological samples in liquids. One could also use side illumination with general AFM substrates for imaging dry samples. The deflection signal of the cantilever is detected by a built-in position-sensitive detector (PSD) and is monitored in real time. IR-induced thermal expansion signals are extracted from the deflection waveform with various methods according to used AFM operation modes.[67]

PTIR with Contact Mode. The force-detected AFM+IR was pioneered by Dazzi and colleagues around 2005 and termed PTIR or contact mode AFM-IR.[11] In PTIR, AFM is operated in contact mode, where a constant tip-sample force is maintained in a feedback loop. After an IR pulse hits the tip-sample area and induces photothermal expansion, the cantilever deflection (ringdowns) is recorded and processed with a fast Fourier transform (FFT) to produce PTIR signals. Thanks to large IR cross sections and highly sensitive cantilevers, PTIR can work with uncoated AFM tips.[14] To further enhance the detection sensitivity to the monolayer level, gold-coated AFM tips are utilized together with resonance-enhanced PTIR. A train of IR pulses with a

https://doi.org/10.1021/cbmi.3c00004
Chem. Biomed. Imaging 2023, 1, 3−17

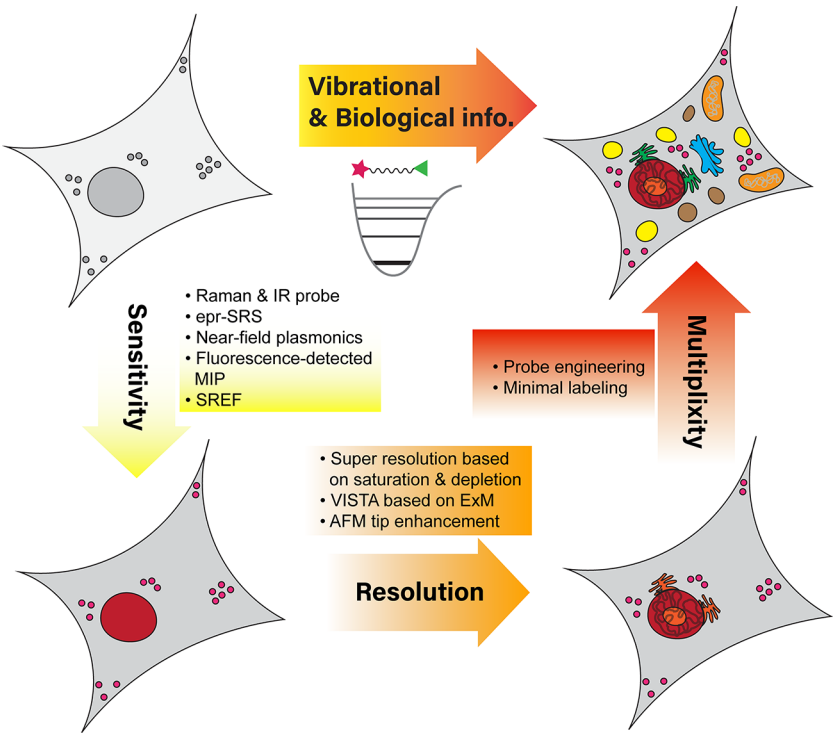

Figure 6. Applying vibrational microscopies to accommodate bioimaging needs. General strategies of increasing sensitivity, improving resolution, and achieving multiplexity by minimal labeling produce different levels of vibrational information that can be interpreted as meaningful biological information. Advancements in SRS, CARS, MIP, and force-detected AFM+IR enable each strategy.

repetition rate that matches one of the cantilever's mechanical eigenmodes is used to enhance photothermal expansions.[99] Resonance-enhanced PTIR has successfully obtained spectral information (e.g., amide bands) for secondary structures from a single thyroglobulin protein deposited on the gold substrate[100] (Figure 5b,c). The high sensitivity brought by the cantilever's resonant enhancement has also enabled PTIR operation in water for biomolecules.[101,102] In contrast to the resonance enhancement, Kenkel et al. used a null-deflection method and optimized IR illumination angles with respect to the tip apex to remove nonchemical backgrounds and increased the sensitivity further.[103] As a result, chemical imaging of the ultrastructure of mammalian cells was achieved, revealing intrinsic biomolecular species with nanoscale resolution (Figure 5e).

PiFM and Tapping AFM-IR. Drawbacks of PTIR mainly come from the contact mode operation: a stable AFM contact mode feedback requires the tip-sample contact all the time, but IR-induced photothermal expansions inevitably push the tip and cantilever to oscillate. Therefore, the scan speed is usually kept low in PTIR for imaging to attenuate the feedback instability. PTIR typically has a resolution of ∼50 nm and tends to cause sample damage and tip scratch.[104] Contact mode is also incompatible with uneven and sticky samples, making it challenging to study mammalian cells and tissues. These issues can be alleviated in tapping mode AFM. In tapping mode, the cantilever oscillates at its mechanical resonance frequency above the surface, and the tip-sample interaction is minimized. Therefore, tapping mode causes minor sample and tip damage and supersedes the contact mode in measuring rough and sticky samples with a higher resolution of 10−20 nm and a faster scanning speed.[105]

Two similar IR methods were established with tapping mode: photoinduced force microscopy (PiFM)[12] and tapping AFM-IR.[106] The signal in PiFM was thought to originate from tip-induced dipole interactions, but later evidence showed that contributions from photothermal expansion are not trivial.[107−109] Both PiFM and tapping AFM-IR utilized the detection scheme of force heterodyne.[110] In the force heterodyne, the laser repetition rate is adjusted to the difference between the first two eigenmodes of the cantilever ($\Omega_2 - \Omega_1$), and the tapping mode is operated at the second eigenmode frequency (Ω_2, $\Omega_2 \approx 6.3\Omega_1$). Consequently, the "beating" frequency of $\Omega_2 - \Omega_1$ would generate a component at the sideband of $\Omega_2 - (\Omega_2 - \Omega_1)$, which is coincident with Ω_1 and therefore is significantly enhanced due to the high quality factor (Q-factor) of the first eigenmode. In this way, background at $\Omega_2 - \Omega_1$ and Ω_2 is reduced at Ω_1, enabling PiFM to reach monolayer sensitivity with plasmonic enhancements.[111] PiFM and tapping AFM-IR were soon demonstrated to be useful in biological applications ranging from biotoxin identification[112] (Figure 5d) and bacterial cell wall mapping to investigations of drug distribution and drug-loaded nanocarriers.[113]

Despite advantages over contact mode PTIR, it is challenging to implement PiFM and tapping AFM-IR in water for broader bioimaging applications. The force heterodyne detection requires the cantilever to have two well-defined eigenmodes with high Q-factors, which is hard to fulfill in viscous liquid environments.[102]

PFIR with Peak Force Tapping AFM. The peak force tapping (PFT, or pulsed force mode) AFM operation mode fills the gap between the contact and the tapping modes. In PFT mode, the tip-sample distance undergoes engaging-detaching cycles at a much lower frequency (e.g., 1−8 kHz)

https://doi.org/10.1021/cbmi.3c00004
Chem. Biomed. Imaging 2023, 1, 3−17

Table 1. Parameters and Performance of CRS, MIP, and Force-Detected AFM+IR

	CRS microscopy	MIP	Force-detected AFM+IR
Contrast origin	Nonlinear coherent Raman	IR-induced photothermal effects	IR-induced photothermal expansion
Detection scheme	SRL/SRG and CARS, far-field	IR pump + visible/near-IR probe, far-field	IR pump + AFM force probe, near-field
Typical lasers and modulation	Femto or picosecond near-IR OPO, MHz	Nanosecond mid-IR QCL & OPO, kHz	Nanosecond mid-IR QCL & OPO, kHz
Platform	Laser scan or stage scan microscopes	Stage scan and wide-field microscopes	Stage scan AFM
Sample for cell imaging	Live or fixed on coverslips	Live or fixed on IR-transparent coverslips	Immobilized on AFM substrate
3D sectioning	Yes	Yes	No
Typical pixel dwell time and best imaging speed	μs, video-rate	μs to ms, video-rate with wide-field imaging	ms, minutes per frame
Sensitivity	mM for endogenous species; μM for Raman probes; nM for epr-SRS with Raman-active dyes; single-molecule with SREF or plasmonic enhancement	μM to mM	Monolayer and single protein molecule with plasmonic enhancement
Spatial resolution	Diffraction limited; super-resolution with depletion or saturation; ~50−80 nm with VISTA and other ExM strategies	Diffraction limited by the probe beam; super-resolution with high-harmonic demodulation	10~20 nm for PiFM, tapping AFM-IR, and PFIR

than in the tapping mode. The force between the tip and the sample is monitored within each cycle. The maximal tip-sample force during each cycle, named peak force, is used as the feedback set point and accurately maintained at the pN to nN level.[114] PFT retrieves surface mechanical information (e.g., modulus and adhesion) from the short period of tip-sample contact. The PFT operation with small levels of peak force also helps minimize the tip-sample interaction and provides stable and fast scanning for rough and sticky samples with high spatial resolution.[115]

In 2017, PFIR microscopy based on PFT was developed in Xu group.[13] The unique feature distinguishing PFIR from others is simultaneously capturing the quantitative mechanical information, which permits multichannel and correlative imaging in the same field of view. The flexibility of PFT also gives birth to the combination of Kelvin probe force microscopy (KPFM) and PFIR, which opens the door for simultaneous and correlative IR and surface potential imaging on amyloid fibrils[116] (Figure 5g,h). Similar to resonance-enhanced PTIR, a multipulse-driven PFIR scheme was demonstrated to improve the sensitivity.[117] The well-tuned PFT operation enables PFIR to maintain a spatial resolution of ~10 nm across a variety of organic and inorganic samples.[113] For instance, PFIR revealed heterogeneous chemical compositions and nanoscale ultrastructure on the yeast cell wall[118] (Figure 5f). PFIR with a TIR prism was implemented for in-liquid operation and used to monitor zeptomolar click chemistry products on the polymer surface *in situ*.[119] With liquid-phase PFIR, yeast cells were investigated in their native states (Figure 5i). Equipped with nanoscale resolution, high sensitivity, and good biocompatibility, PFIR is progressing toward more discoveries in biological systems with unprecedented details.

CONCLUDING REMARKS AND PERSPECTIVE

As the old saying goes: seeing is believing. Imaging the biosystem with light microscopy has proven to be a powerful way to uncover basic cellular events from complex organisms with minimal perturbations. The emergence of fluorescence microscopy has dramatically expanded our knowledge of biophysics, cell biology, neuroscience, and pharmaceutics, from single organelles to whole animals.[120] In the meantime, the need for vibrational imaging is rapidly growing, as rich chemical information about molecules and structures is contained in their vibrational signatures. The appreciation of vibrational information obtained by Raman and IR in biological systems would provide new scopes to understand how things work and address the limitations of fluorescence microscopy with minimal perturbation and supermultiplexing capabilities. To this end, CRS, MIP, and force-detected AFM +IR are still rapidly evolving with quests for better performances and setting up an expanding toolbox for the future of vibrational bioimaging to uncover complex biology (Figure 6).

The pros and cons of CRS, MIP, and force-detected AFM +IR should be considered with a balanced choice of combined imaging parameters when tackling a specific bioimaging challenge. We summarized and compared parameters relevant to the implementation, performance, and bioimaging applications of the three methods to better inform the choice and further inspire development (Table 1).

The drive for better sensitivity, super-multiplexity, and spatial resolution below the diffraction limit becomes the next improvement focus for far-field CRS and MIP. For better sensitivity and super multiplexity with tens of colors, multiple palettes of engineered Raman dyes were developed, including MARS[59,63] and Carbow[61] series. Similar strategies used in engineering Raman dyes, such as isotope doping and end-capping substitution, could be readily applied to engineering new IR probes for emerging MIP and force-detected AFM+IR applications. The unique advantages of IR probes have been exemplified in mid-IR metabolic imaging with direct IR absorption microscopy.[121]

Advances in fluorescence microscopy also accelerate the development of CRS and MIP. The idea of super-resolution CRS based on depletion and saturation traces back to stimulated emission depletion (STED) microscopy[122] and saturated structured illumination microscopy[123] (SSIM). The <100 nm resolution obtained by label-free VISTA results from combining SRS with modified sample treatments used in ExM. Likewise, Shi et al. recently used another expansion protocol to achieve <50 nm resolution.[124] Recent development and investigation of photoswitchable and activatable Raman dyes and proteins[125−127] inspired by the photochromic fluorophores promise the potential of supermultiplex super-resolution imaging. The continuing efforts of absorbing state-of-the-art

https://doi.org/10.1021/cbmi.3c00004
Chem. Biomed. Imaging 2023, 1, 3−17

fluorescence techniques will aid vibrational microscopy to keep pace with the growing bioimaging need.

Fluorescence generated by Raman and IR-active fluorescent molecules offers both bond-selective imaging and high sensitivity. By detecting double-resonance fluorescence enabled by the SRS pump and Stokes, SREF imaging has reached single-molecule sensitivity without near-field plasmonic enhancements.[76] Correspondingly, fluorescence-detected MIP microscopy achieves much higher imaging sensitivity than the regular MIP.[89,90] Recently, fluorescence-encoded infrared (FEIR) spectroscopy has shown single-molecule sensitivity in solution.[128] The apparent "drawback" of using fluorescence detection is the requirement of fluorescent molecules, which renders vibrational imaging no longer label-free. However, such vibrational modality gains a much higher specificity with high functional information throughput from encompassing rational labeling strategies, which tag and highlight targeted biomolecules from complex biosystem environments with the potential for further vibrational multiplexing and sensing.

Scientists have devoted many efforts to developing far-field super-resolution microscopy. Meanwhile, sub-50 nm resolution is routinely achievable for the near-field force-detected AFM +IR. What prevents AFM+IR from wide bioimaging applications are mostly intrinsic limitations of AFM. AFM only scans the top surface and thus has no sectioning capability for thick specimens. To address this issue, a streamlined slice-and-view method could be used to obtain volumetric images of biological systems.[129] Another limitation is the imaging speed. Compared to laser scans in CRS microscopy, AFM stage scan has a much slower frame time from minutes to hours, leaving many dynamic biological processes[130] untraceable. One possible solution is the incorporation of IR with high-speed AFM (HS-AFM), which uses a short cantilever with a much higher mechanical frequency (e.g., in MHz).[131] HS-AFM can provide video-rate imaging speed, but its combination with IR-photothermal detection is challenging and may require a highly specialized AFM probe.

The development of broadband and multiplexed SRS and CARS methods has increased imaging speed and expanded the volume of obtainable vibrational information. For the point-scan MIP and force-detected AFM+IR, hyperspectral data can be constructed sequentially using multiple laser lines in parallel[132,133] or a fast-tunable QCL. On the other hand, implementations of broadband MIP and force-detected AFM +IR are of increasing interest. The combination of AFM+IR with broadband laser and Fourier-transformed schemes has recently opened doors for ultrafast IR spectro-microscopy at the nanoscale.[134,135] These techniques are expected to not only increase the imaging speed and multiplexity but also uncover structural and temporal biological information, such as protein conformation and dynamics which are unachievable with linear spectroscopic methods.

In summary, developments of three types of growing vibrational microscopy, CRS, MIP, and force-detected AFM +IR, were discussed with a focus on bioimaging applications. Each technique here has unique advantages for spectro-microscopic analysis, with afore-discussed issues that could significantly be alleviated from learning the developmental trajectory from each other. Since birth, CRS and MIP have been aimed at vibrational bioimaging. Besides providing complementary vibrational information, their imaging performance today is close to state-of-the-art fluorescence microscopy, thanks to continuous efforts to improve the sensitivity, spatial and temporal resolution, and devising proper matching molecular strategies for functional imaging (e.g., super-multiplexity) and sensing. In contrast, although force-detected AFM+IR has already demonstrated itself as a powerful technique to reach <50 nm resolution routinely, it is still on the way toward fully accommodating general bioimaging needs. Fortunately, technical evolutions such as a well-tuned PFT mode, fast-tuning QCL, and HS-AFM indicate the next breakthrough in force-detected AFM+IR may be near the corner. With all three methods and ongoing developments, the road toward the future of vibrational bioimaging will be paved with exciting innovations and groundbreaking discoveries.

AUTHOR INFORMATION

Corresponding Author

Lu Wei − *Division of Chemistry and Chemical Engineering, California Institute of Technology, Pasadena, California 91125, United States;* orcid.org/0000-0001-9170-2283; Email: lwei@caltech.edu

Authors

Haomin Wang − *Division of Chemistry and Chemical Engineering, California Institute of Technology, Pasadena, California 91125, United States;* orcid.org/0000-0001-7193-8651

Dongkwan Lee − *Division of Chemistry and Chemical Engineering, California Institute of Technology, Pasadena, California 91125, United States;* orcid.org/0000-0001-6091-1349

Complete contact information is available at: https://pubs.acs.org/10.1021/cbmi.3c00004

Notes

The authors declare no competing financial interest.

ACKNOWLEDGMENTS

The authors would like to thank the support from NIH Director's New Innovator Award, DP2 GM140919-01.

REFERENCES

(1) Herzberg, G. *Molecular spectra and molecular structure: Infrared and Raman spectra of polyatomic molecules*; Van Nostrand Reinhold, 1945; Vol. 2.

(2) Lakowicz, J. R. *Principles of Fluorescence Spectroscopy*, 3rd ed.; Springer: New York, 2006.

(3) Shen, Y.; Hu, F.; Min, W. Raman Imaging of Small Biomolecules. *Annu. Rev. Biophys.* **2019**, *48* (1), 347−369.

(4) Ma, J.; Pazos, I. M.; Zhang, W.; Culik, R. M.; Gai, F. Site-Specific Infrared Probes of Proteins. *Annu. Rev. Phys. Chem.* **2015**, *66* (1), 357−377.

(5) Cheng, J. X.; Xie, X. S. *Coherent Raman Scattering Microscopy*; CRC Press, 2012.

(6) Whinnery, J. R. Review of Some Photothermal Effects. *Amazing Light* **1996**, 643−649.

(7) Zhang, D.; Li, C.; Zhang, C.; Slipchenko, M. N.; Eakins, G.; Cheng, J.-X. Depth-resolved mid-infrared photothermal imaging of living cells and organisms with submicrometer spatial resolution. *Sci. Adv.* **2016**, *2* (9), e1600521.

(8) Li, Z.; Aleshire, K.; Kuno, M.; Hartland, G. V. Super-Resolution Far-Field Infrared Imaging by Photothermal Heterodyne Imaging. *J. Phys. Chem. B* **2017**, *121* (37), 8838−8846.

(9) Maier, S. A. *Plasmonics: fundamentals and applications*; Springer Science & Business Media, 2007.

(10) Wachter, E. A.; Thundat, T. Micromechanical sensors for chemical and physical measurements. *Rev. Sci. Instrum.* **1995**, *66* (6), 3662−3667.
(11) Dazzi, A.; Prazeres, R.; Glotin, F.; Ortega, J. M. Local infrared microspectroscopy with subwavelength spatial resolution with an atomic force microscope tip used as a photothermal sensor. *Opt. Lett.* **2005**, *30* (18), 2388−2390.
(12) Nowak, D.; Morrison, W.; Wickramasinghe, H. K.; Jahng, J.; Potma, E.; Wan, L.; Ruiz, R.; Albrecht, T. R.; Schmidt, K.; Frommer, J.; Sanders, D. P.; Park, S. Nanoscale chemical imaging by photoinduced force microscopy. *Sci. Adv.* **2016**, *2* (3), e1501571.
(13) Wang, L.; Wang, H.; Wagner, M.; Yan, Y.; Jakob, D. S.; Xu, X. G. Nanoscale simultaneous chemical and mechanical imaging via peak force infrared microscopy. *Sci. Adv.* **2017**, *3* (6), e1700255.
(14) Dazzi, A.; Prater, C. B. AFM-IR: Technology and Applications in Nanoscale Infrared Spectroscopy and Chemical Imaging. *Chem. Rev.* **2017**, *117* (7), 5146−5173.
(15) Prince, R. C.; Frontiera, R. R.; Potma, E. O. Stimulated Raman Scattering: From Bulk to Nano. *Chem. Rev.* **2017**, *117* (7), 5070−5094.
(16) Maiman, T. H. Stimulated Optical Radiation in Ruby. *Nature* **1960**, *187* (4736), 493−494.
(17) Duncan, M. D.; Reintjes, J.; Manuccia, T. J. Scanning coherent anti-Stokes Raman microscope. *Opt. Lett.* **1982**, *7* (8), 350−352.
(18) Zumbusch, A.; Holtom, G. R.; Xie, X. S. Three-Dimensional Vibrational Imaging by Coherent Anti-Stokes Raman Scattering. *Phys. Rev. Lett.* **1999**, *82* (20), 4142−4145.
(19) Evans, C. L.; Potma, E. O.; Puoris'haag, M.; Côté, D.; Lin, C. P.; Xie, X. S. Chemical imaging of tissue in vivo with video-rate coherent anti-Stokes Raman scattering microscopy. *Proc. Natl. Acad. Sci. U. S. A.* **2005**, *102* (46), 16807−16812.
(20) Ploetz, E.; Laimgruber, S.; Berner, S.; Zinth, W.; Gilch, P. Femtosecond stimulated Raman microscopy. *Appl. Phys. B: Laser Opt.* **2007**, *87* (3), 389−393.
(21) Freudiger, C. W.; Min, W.; Saar, B. G.; Lu, S.; Holtom, G. R.; He, C.; Tsai, J. C.; Kang, J. X.; Xie, X. S. Label-Free Biomedical Imaging with High Sensitivity by Stimulated Raman Scattering Microscopy. *Science* **2008**, *322* (5909), 1857−1861.
(22) Nandakumar, P.; Kovalev, A.; Volkmer, A. Vibrational imaging based on stimulated Raman scattering microscopy. *New J. Phys.* **2009**, *11* (3), No. 033026.
(23) Ozeki, Y.; Dake, F.; Kajiyama, S. i.; Fukui, K.; Itoh, K. Analysis and experimental assessment of the sensitivity of stimulated Raman scattering microscopy. *Opt. Express* **2009**, *17* (5), 3651−3658.
(24) Saar, B. G.; Freudiger, C. W.; Reichman, J.; Stanley, C. M.; Holtom, G. R.; Xie, X. S. Video-Rate Molecular Imaging in Vivo with Stimulated Raman Scattering. *Science* **2010**, *330* (6009), 1368−1370.
(25) Cheng, J.-X.; Min, W.; Ozeki, Y.; Polli, D. *Stimulated Raman Scattering Microscopy: Techniques and Applications*, 1st ed.; Elsevier, 2021.
(26) Min, W.; Freudiger, C. W.; Lu, S.; Xie, X. S. Coherent Nonlinear Optical Imaging: Beyond Fluorescence Microscopy. *Annu. Rev. Phys. Chem.* **2011**, *62* (1), 507−530.
(27) Polli, D.; Kumar, V.; Valensise, C. M.; Marangoni, M.; Cerullo, G. Broadband Coherent Raman Scattering Microscopy. *Laser Photonics Rev.* **2018**, *12* (9), 1800020.
(28) Zhang, C.; Cheng, J.-X. Perspective: Coherent Raman scattering microscopy, the future is bright. *APL Photonics* **2018**, *3* (9), No. 090901.
(29) Zhang, D.; Wang, P.; Slipchenko, M. N.; Cheng, J.-X. Fast Vibrational Imaging of Single Cells and Tissues by Stimulated Raman Scattering Microscopy. *Acc. Chem. Res.* **2014**, *47* (8), 2282−2290.
(30) Wei, L.; Hu, F.; Chen, Z.; Shen, Y.; Zhang, L.; Min, W. Live-Cell Bioorthogonal Chemical Imaging: Stimulated Raman Scattering Microscopy of Vibrational Probes. *Acc. Chem. Res.* **2016**, *49* (8), 1494−1502.
(31) Hu, F.; Shi, L.; Min, W. Biological imaging of chemical bonds by stimulated Raman scattering microscopy. *Nat. Methods* **2019**, *16* (9), 830−842.
(32) Camp, C. H., Jr; Lee, Y. J.; Heddleston, J. M.; Hartshorn, C. M.; Walker, A. R. H.; Rich, J. N.; Lathia, J. D.; Cicerone, M. T. High-speed coherent Raman fingerprint imaging of biological tissues. *Nat. Photonics* **2014**, *8* (8), 627−634.
(33) Fu, D.; Zhou, J.; Zhu, W. S.; Manley, P. W.; Wang, Y. K.; Hood, T.; Wylie, A.; Xie, X. S. Imaging the intracellular distribution of tyrosine kinase inhibitors in living cells with quantitative hyperspectral stimulated Raman scattering. *Nat. Chem.* **2014**, *6* (7), 614−622.
(34) Cheng, J.-X.; Xie, X. S. Vibrational spectroscopic imaging of living systems: An emerging platform for biology and medicine. *Science* **2015**, *350* (6264), aaa8870.
(35) Lu, F.-K.; Basu, S.; Igras, V.; Hoang, M. P.; Ji, M.; Fu, D.; Holtom, G. R.; Neel, V. A.; Freudiger, C. W.; Fisher, D. E.; Xie, X. S. Label-free DNA imaging in vivo with stimulated Raman scattering microscopy. *Proc. Natl. Acad. Sci. U. S. A.* **2015**, *112* (37), 11624−11629.
(36) Orringer, D. A.; Pandian, B.; Niknafs, Y. S.; Hollon, T. C.; Boyle, J.; Lewis, S.; Garrard, M.; Hervey-Jumper, S. L.; Garton, H. J. L.; Maher, C. O.; Heth, J. A.; Sagher, O.; Wilkinson, D. A.; Snuderl, M.; Venneti, S.; Ramkissoon, S. H.; McFadden, K. A.; Fisher-Hubbard, A.; Lieberman, A. P.; Johnson, T. D.; Xie, X. S.; Trautman, J. K.; Freudiger, C. W.; Camelo-Piragua, S. Rapid intraoperative histology of unprocessed surgical specimens via fibre-laser-based stimulated Raman scattering microscopy. *Nat. Biomed. Eng.* **2017**, *1* (2), No. 0027.
(37) Cheng, J.-x.; Volkmer, A.; Book, L. D.; Xie, X. S. Multiplex Coherent Anti-Stokes Raman Scattering Microspectroscopy and Study of Lipid Vesicles. *J. Phys. Chem. B* **2002**, *106* (34), 8493−8498.
(38) Müller, M.; Schins, J. M. Imaging the Thermodynamic State of Lipid Membranes with Multiplex CARS Microscopy. *J. Phys. Chem. B* **2002**, *106* (14), 3715−3723.
(39) Kong, L.; Ji, M.; Holtom, G. R.; Fu, D.; Freudiger, C. W.; Xie, X. S. Multicolor stimulated Raman scattering microscopy with a rapidly tunable optical parametric oscillator. *Opt. Lett.* **2013**, *38* (2), 145−147.
(40) Ozeki, Y.; Umemura, W.; Otsuka, Y.; Satoh, S.; Hashimoto, H.; Sumimura, K.; Nishizawa, N.; Fukui, K.; Itoh, K. High-speed molecular spectral imaging of tissue with stimulated Raman scattering. *Nat. Photonics* **2012**, *6* (12), 845−851.
(41) Liao, C.-S.; Wang, P.; Wang, P.; Li, J.; Lee, H. J.; Eakins, G.; Cheng, J.-X. Spectrometer-free vibrational imaging by retrieving stimulated Raman signal from highly scattered photons. *Sci. Adv.* **2015**, *1* (9), e1500738.
(42) Zhang, C.; Huang, K.-C.; Rajwa, B.; Li, J.; Yang, S.; Lin, H.; Liao, C.-s.; Eakins, G.; Kuang, S.; Patsekin, V.; Robinson, J. P.; Cheng, J.-X. Stimulated Raman scattering flow cytometry for label-free single-particle analysis. *Optica* **2017**, *4* (1), 103−109.
(43) Hellerer, T.; Enejder, A. M. K.; Zumbusch, A. Spectral focusing: High spectral resolution spectroscopy with broad-bandwidth laser pulses. *Appl. Phys. Lett.* **2004**, *85* (1), 25−27.
(44) Fu, D.; Holtom, G.; Freudiger, C.; Zhang, X.; Xie, X. S. Hyperspectral Imaging with Stimulated Raman Scattering by Chirped Femtosecond Lasers. *J. Phys. Chem. B* **2013**, *117* (16), 4634−4640.
(45) Li, J.; Condello, S.; Thomes-Pepin, J.; Ma, X.; Xia, Y.; Hurley, T. D.; Matei, D.; Cheng, J.-X. Lipid Desaturation Is a Metabolic Marker and Therapeutic Target of Ovarian Cancer Stem Cells. *Cell Stem Cell* **2017**, *20* (3), 303−314.e5.
(46) Silva, W. R.; Graefe, C. T.; Frontiera, R. R. Toward Label-Free Super-Resolution Microscopy. *ACS Photonics* **2016**, *3* (1), 79−86.
(47) Yonemaru, Y.; Palonpon, A. F.; Kawano, S.; Smith, N. I.; Kawata, S.; Fujita, K. Super-Spatial- and -Spectral-Resolution in Vibrational Imaging via Saturated Coherent Anti-Stokes Raman Scattering. *Phys. Rev. Appl.* **2015**, *4* (1), No. 014010.
(48) Gong, L.; Zheng, W.; Ma, Y.; Huang, Z. Saturated Stimulated-Raman-Scattering Microscopy for Far-Field Superresolution Vibrational Imaging. *Phys. Rev. Appl.* **2019**, *11* (3), No. 034041.
(49) Gong, L.; Zheng, W.; Ma, Y.; Huang, Z. Higher-order coherent anti-Stokes Raman scattering microscopy realizes label-free super-resolution vibrational imaging. *Nat. Photonics* **2020**, *14* (2), 115−122.

https://doi.org/10.1021/cbmi.3c00004
Chem. Biomed. Imaging 2023, 1, 3−17

(50) Chen, F.; Tillberg, P. W.; Boyden, E. S. Expansion microscopy. *Science* **2015**, *347* (6221), 543−548.
(51) Qian, C.; Miao, K.; Lin, L.-E.; Chen, X.; Du, J.; Wei, L. Super-resolution label-free volumetric vibrational imaging. *Nat. Commun.* **2021**, *12* (1), 3648.
(52) Lin, L.-E.; Miao, K.; Qian, C.; Wei, L. High spatial-resolution imaging of label-free in vivo protein aggregates by VISTA. *Analyst* **2021**, *146* (13), 4135−4145.
(53) Wei, L.; Hu, F.; Shen, Y.; Chen, Z.; Yu, Y.; Lin, C.-C.; Wang, M. C.; Min, W. Live-cell imaging of alkyne-tagged small biomolecules by stimulated Raman scattering. *Nat. Methods* **2014**, *11* (4), 410−412.
(54) Wei, L.; Yu, Y.; Shen, Y.; Wang, M. C.; Min, W. Vibrational imaging of newly synthesized proteins in live cells by stimulated Raman scattering microscopy. *Proc. Natl. Acad. Sci. U. S. A.* **2013**, *110* (28), 11226−11231.
(55) Miao, K.; Wei, L. Live-Cell Imaging and Quantification of PolyQ Aggregates by Stimulated Raman Scattering of Selective Deuterium Labeling. *ACS Cent. Sci.* **2020**, *6* (4), 478−486.
(56) Chen, Z.; Paley, D. W.; Wei, L.; Weisman, A. L.; Friesner, R. A.; Nuckolls, C.; Min, W. Multicolor Live-Cell Chemical Imaging by Isotopically Edited Alkyne Vibrational Palette. *J. Am. Chem. Soc.* **2014**, *136* (22), 8027−8033.
(57) Maier, W.; Dörr, F. Some Results of Resonance Raman Spectroscopy. *Appl. Spectrosc.* **1960**, *14* (1), 1−3.
(58) Wei, L.; Min, W. Electronic Preresonance Stimulated Raman Scattering Microscopy. *J. Phys. Chem. Lett.* **2018**, *9* (15), 4294−4301.
(59) Wei, L.; Chen, Z.; Shi, L.; Long, R.; Anzalone, A. V.; Zhang, L.; Hu, F.; Yuste, R.; Cornish, V. W.; Min, W. Super-multiplex vibrational imaging. *Nature* **2017**, *544* (7651), 465−470.
(60) Zhao, Z.; Chen, C.; Wei, S.; Xiong, H.; Hu, F.; Miao, Y.; Jin, T.; Min, W. Ultra-bright Raman dots for multiplexed optical imaging. *Nat. Commun.* **2021**, *12* (1), 1305.
(61) Hu, F.; Zeng, C.; Long, R.; Miao, Y.; Wei, L.; Xu, Q.; Min, W. Supermultiplexed optical imaging and barcoding with engineered polyynes. *Nat. Methods* **2018**, *15* (3), 194−200.
(62) Miao, Y.; Qian, N.; Shi, L.; Hu, F.; Min, W. 9-Cyanopyronin probe palette for super-multiplexed vibrational imaging. *Nat. Commun.* **2021**, *12* (1), 4518.
(63) Shi, L.; Wei, M.; Miao, Y.; Qian, N.; Shi, L.; Singer, R. A.; Benninger, R. K. P.; Min, W. Highly-multiplexed volumetric mapping with Raman dye imaging and tissue clearing. *Nat. Biotechnol.* **2022**, *40* (3), 364−373.
(64) Stöckle, R. M.; Suh, Y. D.; Deckert, V.; Zenobi, R. Nanoscale chemical analysis by tip-enhanced Raman spectroscopy. *Chem. Phys. Lett.* **2000**, *318* (1), 131−136.
(65) Stiles, P. L.; Dieringer, J. A.; Shah, N. C.; Van Duyne, R. P. Surface-Enhanced Raman Spectroscopy. *Annu. Rev. Anal. Chem.* **2008**, *1* (1), 601−626.
(66) Hutter, E.; Fendler, J. H. Exploitation of Localized Surface Plasmon Resonance. *Adv. Mater.* **2004**, *16* (19), 1685−1706.
(67) Kurouski, D.; Dazzi, A.; Zenobi, R.; Centrone, A. Infrared and Raman chemical imaging and spectroscopy at the nanoscale. *Chem. Soc. Rev.* **2020**, *49* (11), 3315−3347.
(68) Lee, J.; Crampton, K. T.; Tallarida, N.; Apkarian, V. A. Visualizing vibrational normal modes of a single molecule with atomically confined light. *Nature* **2019**, *568* (7750), 78−82.
(69) Lipiec, E.; Kaderli, J.; Kobierski, J.; Riek, R.; Skirlińska-Nosek, K.; Sofińska, K.; Szymoński, M.; Zenobi, R. Nanoscale Hyperspectral Imaging of Amyloid Secondary Structures in Liquid. *Angew. Chem., Int. Ed.* **2021**, *60* (9), 4545−4550.
(70) Mrđenović, D.; Ge, W.; Kumar, N.; Zenobi, R. Nanoscale Chemical Imaging of Human Cell Membranes Using Tip-Enhanced Raman Spectroscopy. *Angew. Chem., Int. Ed.* **2022**, *61* (43), e202210288.
(71) Zong, C.; Premasiri, R.; Lin, H.; Huang, Y.; Zhang, C.; Yang, C.; Ren, B.; Ziegler, L. D.; Cheng, J.-X. Plasmon-enhanced stimulated Raman scattering microscopy with single-molecule detection sensitivity. *Nat. Commun.* **2019**, *10* (1), 5318.
(72) Zhang, Y.; Zhen, Y.-R.; Neumann, O.; Day, J. K.; Nordlander, P.; Halas, N. J. Coherent anti-Stokes Raman scattering with single-molecule sensitivity using a plasmonic Fano resonance. *Nat. Commun.* **2014**, *5* (1), 4424.
(73) Yampolsky, S.; Fishman, D. A.; Dey, S.; Hulkko, E.; Banik, M.; Potma, E. O.; Apkarian, V. A. Seeing a single molecule vibrate through time-resolved coherent anti-Stokes Raman scattering. *Nat. Photonics* **2014**, *8* (8), 650−656.
(74) Wickramasinghe, H. K.; Chaigneau, M.; Yasukuni, R.; Picardi, G.; Ossikovski, R. Billion-Fold Increase in Tip-Enhanced Raman Signal. *ACS Nano* **2014**, *8* (4), 3421−3426.
(75) Lee, S. H.; Nguyen, D. C.; Wright, J. C. Double Resonance Excitation of Fluorescence by Stimulated Raman Scattering. *Appl. Spectrosc.* **1983**, *37* (5), 472−474.
(76) Xiong, H.; Shi, L.; Wei, L.; Shen, Y.; Long, R.; Zhao, Z.; Min, W. Stimulated Raman excited fluorescence spectroscopy and imaging. *Nat. Photonics* **2019**, *13* (6), 412−417.
(77) Xiong, H.; Min, W. Combining the best of two worlds: Stimulated Raman excited fluorescence. *J. Chem. Phys.* **2020**, *153* (21), 210901.
(78) McCann, P. C.; Hiramatsu, K.; Goda, K. Highly Sensitive Low-Frequency Time-Domain Raman Spectroscopy via Fluorescence Encoding. *J. Phys. Chem. Lett.* **2021**, *12* (32), 7859−7865.
(79) Pavlovetc, I. M.; Aleshire, K.; Hartland, G. V.; Kuno, M. Approaches to mid-infrared, super-resolution imaging and spectroscopy. *Phys. Chem. Chem. Phys.* **2020**, *22* (8), 4313−4325.
(80) Bai, Y.; Yin, J.; Cheng, J.-X. Bond-selective imaging by optically sensing the mid-infrared photothermal effect. *Sci. Adv.* **2021**, *7* (20), eabg1559.
(81) Li, X.; Zhang, D.; Bai, Y.; Wang, W.; Liang, J.; Cheng, J.-X. Fingerprinting a Living Cell by Raman Integrated Mid-Infrared Photothermal Microscopy. *Anal. Chem.* **2019**, *91* (16), 10750−10756.
(82) Fu, P.; Cao, W.; Chen, T.; Huang, X.; Le, T.; Zhu, S.; Wang, D.-W.; Lee, H. J.; Zhang, D. Super-resolution imaging of non-fluorescent molecules by photothermal relaxation localization microscopy. *Nat. Photonics* **2023**.
(83) Adhikari, S.; Spaeth, P.; Kar, A.; Baaske, M. D.; Khatua, S.; Orrit, M. Photothermal Microscopy: Imaging the Optical Absorption of Single Nanoparticles and Single Molecules. *ACS Nano* **2020**, *14* (12), 16414−16445.
(84) Lee, E. S.; Lee, J. Y. Nonlinear optical infrared microscopy with chemical specificity. *Appl. Phys. Lett.* **2009**, *94* (26), 261101.
(85) Lee, E. S.; Lee, J. Y. High resolution cellular imaging with nonlinear optical infrared microscopy. *Opt. Express* **2011**, *19* (2), 1378−1384.
(86) Lim, J. M.; Park, C.; Park, J.-S.; Kim, C.; Chon, B.; Cho, M. Cytoplasmic Protein Imaging with Mid-Infrared Photothermal Microscopy: Cellular Dynamics of Live Neurons and Oligodendrocytes. *J. Phys. Chem. Lett.* **2019**, *10* (11), 2857−2861.
(87) Bai, Y.; Zhang, D.; Lan, L.; Huang, Y.; Maize, K.; Shakouri, A.; Cheng, J.-X. Ultrafast chemical imaging by widefield photothermal sensing of infrared absorption. *Sci. Adv.* **2019**, *5* (7), eaav7127.
(88) Schnell, M.; Mittal, S.; Falahkheirkhah, K.; Mittal, A.; Yeh, K.; Kenkel, S.; Kajdacsy-Balla, A.; Carney, P. S.; Bhargava, R. All-digital histopathology by infrared-optical hybrid microscopy. *Proc. Natl. Acad. Sci. U. S. A.* **2020**, *117* (7), 3388−3396.
(89) Li, M.; Razumtcev, A.; Yang, R.; Liu, Y.; Rong, J.; Geiger, A. C.; Blanchard, R.; Pfluegl, C.; Taylor, L. S.; Simpson, G. J. Fluorescence-Detected Mid-Infrared Photothermal Microscopy. *J. Am. Chem. Soc.* **2021**, *143* (29), 10809−10815.
(90) Zhang, Y.; Zong, H.; Zong, C.; Tan, Y.; Zhang, M.; Zhan, Y.; Cheng, J.-X. Fluorescence-Detected Mid-Infrared Photothermal Microscopy. *J. Am. Chem. Soc.* **2021**, *143* (30), 11490−11499.
(91) Binnig, G.; Rohrer, H.; Gerber, C.; Weibel, E. 7 × 7 Reconstruction on Si(111) Resolved in Real Space. *Phys. Rev. Lett.* **1983**, *50* (2), 120−123.
(92) Binnig, G.; Quate, C. F.; Gerber, C. Atomic Force Microscope. *Phys. Rev. Lett.* **1986**, *56* (9), 930−933.

https://doi.org/10.1021/cbmi.3c00004
Chem. Biomed. Imaging 2023, 1, 3−17

(93) Rugar, D.; Hansma, P. Atomic force microscopy. *Phys. Today* **1990**, *43* (10), 23−30.
(94) Binnig, G.; Gerber, C.; Stoll, E.; Albrecht, T. R.; Quate, C. F. Atomic Resolution with Atomic Force Microscope. *EPL* **1987**, *3* (12), 1281−1286.
(95) Kumar, N.; Weckhuysen, B. M.; Wain, A. J.; Pollard, A. J. Nanoscale chemical imaging using tip-enhanced Raman spectroscopy. *Nat. Protoc.* **2019**, *14* (4), 1169−1193.
(96) Knoll, B.; Keilmann, F. Near-field probing of vibrational absorption for chemical microscopy. *Nature* **1999**, *399* (6732), 134−137.
(97) Chen, X.; Hu, D.; Mescall, R.; You, G.; Basov, D. N.; Dai, Q.; Liu, M. Modern Scattering-Type Scanning Near-Field Optical Microscopy for Advanced Material Research. *Adv. Mater.* **2019**, *31* (24), 1804774.
(98) Ramer, G.; Aksyuk, V. A.; Centrone, A. Quantitative Chemical Analysis at the Nanoscale Using the Photothermal Induced Resonance Technique. *Anal. Chem.* **2017**, *89* (24), 13524−13531.
(99) Lu, F.; Jin, M.; Belkin, M. A. Tip-enhanced infrared nanospectroscopy via molecular expansion force detection. *Nat. Photonics* **2014**, *8* (4), 307−312.
(100) Ruggeri, F. S.; Mannini, B.; Schmid, R.; Vendruscolo, M.; Knowles, T. P. J. Single molecule secondary structure determination of proteins through infrared absorption nanospectroscopy. *Nat. Commun.* **2020**, *11* (1), 2945.
(101) Ramer, G.; Ruggeri, F. S.; Levin, A.; Knowles, T. P. J.; Centrone, A. Determination of Polypeptide Conformation with Nanoscale Resolution in Water. *ACS Nano* **2018**, *12* (7), 6612−6619.
(102) Jin, M.; Lu, F.; Belkin, M. A. High-sensitivity infrared vibrational nanospectroscopy in water. *Light: Sci. Appl.* **2017**, *6* (7), e17096−e17096.
(103) Kenkel, S.; Gryka, M.; Chen, L.; Confer, M. P.; Rao, A.; Robinson, S.; Prasanth, K. V.; Bhargava, R. Chemical imaging of cellular ultrastructure by null-deflection infrared spectroscopic measurements. *Proc. Natl. Acad. Sci. U. S. A.* **2022**, *119* (47), e2210516119.
(104) Johnson, K. L.; Woodhouse, J. Stick−slip motion in the atomic force microscope. *Tribol. Lett.* **1998**, *5* (2), 155−160.
(105) Prater, C.; Maivald, P.; Kjoller, K.; Heaton, M. *TappingMode imaging applications and technology*; Bruker: Santa Barbara, California, USA, 1995.
(106) Mathurin, J.; Pancani, E.; Deniset-Besseau, A.; Kjoller, K.; Prater, C. B.; Gref, R.; Dazzi, A. How to unravel the chemical structure and component localization of individual drug-loaded polymeric nanoparticles by using tapping AFM-IR. *Analyst* **2018**, *143* (24), 5940−5949.
(107) Jahng, J.; Potma, E. O.; Lee, E. S. Tip-Enhanced Thermal Expansion Force for Nanoscale Chemical Imaging and Spectroscopy in Photoinduced Force Microscopy. *Anal. Chem.* **2018**, *90* (18), 11054−11061.
(108) Wang, L.; Wang, H.; Vezenov, D.; Xu, X. G. Direct Measurement of Photoinduced Force for Nanoscale Infrared Spectroscopy and Chemical-Sensitive Imaging. *J. Phys. Chem. C* **2018**, *122* (41), 23808−23813.
(109) Jahng, J.; Potma, E. O.; Lee, E. S. Nanoscale spectroscopic origins of photoinduced tip-sample force in the midinfrared. *Proc. Natl. Acad. Sci. U. S. A.* **2019**, *116* (52), 26359−26366.
(110) Cuberes, M. T.; Assender, H. E.; Briggs, G. A. D.; Kolosov, O. V. Heterodyne force microscopy of PMMA/rubber nanocomposites: nanomapping of viscoelastic response at ultrasonic frequencies. *J. Phys. D: Appl. Phys.* **2000**, *33* (19), 2347−2355.
(111) Jahng, J.; Son, J. G.; Kim, H.; Park, J.; Lee, T. G.; Lee, E. S. Direct Chemical Imaging of Ligand-Functionalized Single Nanoparticles by Photoinduced Force Microscopy. *J. Phys. Chem. Lett.* **2020**, *11* (14), 5785−5791.
(112) Ji, B.; Kenaan, A.; Gao, S.; Cheng, J.; Cui, D.; Yang, H.; Wang, J.; Song, J. Label-free detection of biotoxins via a photo-induced force infrared spectrum at the single-molecular level. *Analyst* **2019**, *144* (20), 6108−6117.
(113) Wang, H.; Xie, Q.; Xu, X. G. Super-resolution mid-infrared spectro-microscopy of biological applications through tapping mode and peak force tapping mode atomic force microscope. *Adv. Drug Delivery Rev.* **2022**, *180*, 114080.
(114) Pittenger, B.; Erina, N.; Su, C. *Quantitative mechanical property mapping at the nanoscale with PeakForce QNM*; Bruker, 2010.
(115) Li, M.; Xi, N.; Liu, L. Peak force tapping atomic force microscopy for advancing cell and molecular biology. *Nanoscale* **2021**, *13* (18), 8358−8375.
(116) Jakob, D. S.; Wang, H.; Zeng, G.; Otzen, D. E.; Yan, Y.; Xu, X. G. Peak Force Infrared−Kelvin Probe Force Microscopy. *Angew. Chem., Int. Ed.* **2020**, *59* (37), 16083−16090.
(117) Wang, L.; Wagner, M.; Wang, H.; Pau-Sanchez, S.; Li, J.; Edgar, J. H.; Xu, X. G. Revealing Phonon Polaritons in Hexagonal Boron Nitride by Multipulse Peak Force Infrared Microscopy. *Adv. Opt. Mater.* **2020**, *8* (5), 1901084.
(118) Li, W.; Wang, H.; Xu, X. G.; Yu, Y. Simultaneous Nanoscale Imaging of Chemical and Architectural Heterogeneity on Yeast Cell Wall Particles. *Langmuir* **2020**, *36* (22), 6169−6177.
(119) Wang, H.; González-Fialkowski, J. M.; Li, W.; Xie, Q.; Yu, Y.; Xu, X. G. Liquid-Phase Peak Force Infrared Microscopy for Chemical Nanoimaging and Spectroscopy. *Anal. Chem.* **2021**, *93* (7), 3567−3575.
(120) Yuste, R. Fluorescence microscopy today. *Nat. Methods* **2005**, *2* (12), 902−904.
(121) Shi, L.; Liu, X.; Shi, L.; Stinson, H. T.; Rowlette, J.; Kahl, L. J.; Evans, C. R.; Zheng, C.; Dietrich, L. E. P.; Min, W. Mid-infrared metabolic imaging with vibrational probes. *Nat. Methods* **2020**, *17* (8), 844−851.
(122) Hell, S. W.; Wichmann, J. Breaking the diffraction resolution limit by stimulated emission: stimulated-emission-depletion fluorescence microscopy. *Opt. Lett.* **1994**, *19* (11), 780−782.
(123) Gustafsson, M. G. L. Nonlinear structured-illumination microscopy: Wide-field fluorescence imaging with theoretically unlimited resolution. *Proc. Natl. Acad. Sci. U. S. A.* **2005**, *102* (37), 13081−13086.
(124) Shi, L.; Klimas, A.; Gallagher, B.; Cheng, Z.; Fu, F.; Wijesekara, P.; Miao, Y.; Ren, X.; Zhao, Y.; Min, W. Super-Resolution Vibrational Imaging Using Expansion Stimulated Raman Scattering Microscopy. *Adv. Sci.* **2022**, *9* (20), 2200315.
(125) Lee, D.; Qian, C.; Wang, H.; Li, L.; Miao, K.; Du, J.; Shcherbakova, D. M.; Verkhusha, V. V.; Wang, L. V.; Wei, L. Toward photoswitchable electronic pre-resonance stimulated Raman probes. *J. Chem. Phys.* **2021**, *154* (13), 135102.
(126) Shou, J.; Ozeki, Y. Photoswitchable stimulated Raman scattering spectroscopy and microscopy. *Opt. Lett.* **2021**, *46* (9), 2176−2179.
(127) Ao, J.; Fang, X.; Miao, X.; Ling, J.; Kang, H.; Park, S.; Wu, C.; Ji, M. Switchable stimulated Raman scattering microscopy with photochromic vibrational probes. *Nat. Commun.* **2021**, *12* (1), 3089.
(128) Whaley-Mayda, L.; Guha, A.; Penwell, S. B.; Tokmakoff, A. Fluorescence-Encoded Infrared Vibrational Spectroscopy with Single-Molecule Sensitivity. *J. Am. Chem. Soc.* **2021**, *143* (8), 3060−3064.
(129) Kanevche, K.; Burr, D. J.; Nürnberg, D. J.; Hass, P. K.; Elsaesser, A.; Heberle, J. Infrared nanoscopy and tomography of intracellular structures. *Commun. Biol.* **2021**, *4* (1), 1341.
(130) Shamir, M.; Bar-On, Y.; Phillips, R.; Milo, R. SnapShot: Timescales in Cell Biology. *Cell* **2016**, *164* (6), 1302−1302. e1.
(131) Ando, T.; Uchihashi, T.; Kodera, N. High-Speed AFM and Applications to Biomolecular Systems. *Annu. Rev. Biophys.* **2013**, *42* (1), 393−414.
(132) Xie, Q.; Wiemann, J.; Yu, Y.; Xu, X. G. Dual-Color Peak Force Infrared Microscopy. *Anal. Chem.* **2022**, *94* (2), 1425−1431.
(133) Jakob, D. S.; Centrone, A. Visible to Mid-IR Spectromicroscopy with Top-Down Illumination and Nanoscale (≈10 nm) Resolution. *Anal. Chem.* **2022**, *94* (45), 15564−15569.
(134) Xie, Q.; Xu, X. G. Fourier-Transform Atomic Force Microscope-Based Photothermal Infrared Spectroscopy with Broadband Source. *Nano Lett.* **2022**, *22* (22), 9174−9180.

(135) Bohlmann Kunz, M.; Podorova, Y.; Armstrong, Z. T.; Zanni, M. T. Time-Domain Photothermal AFM Spectroscopy via Femtosecond Pulse Shaping. *Anal. Chem.* **2022**, *94* (36), 12374−12382.

https://doi.org/10.1021/cbmi.3c00004
Chem. Biomed. Imaging 2023, 1, 3−17